11-17-2016

Analysis of Aerosol Absorption Properties and Transport Over North Africa and the Middle East Using AERONET Data

Ashraf Farahat
King Fahd University of Petroleum and Minerals, Saudi Arabia

Hesham el-Askary
Chapman University, elaskary@chapman.edu

Peter Adetokunbo
State University of New York at Buffalo

Abu-Tharr Fuad
Qatar University

Recommended Citation

Farahat, A., El-Askary, H., Adetokunbo, P., and Fuad, A.-T.: Analysis of aerosol absorption properties and transport over North Africa and the Middle East using AERONET data, *Ann. Geophys.*, 34, 1031-1044, doi:10.5194/angeo-34-1031-2016, 2016.

Analysis of Aerosol Absorption Properties and Transport Over North Africa and the Middle East Using AERONET Data

Ann. Geophys., 34, 1031–1044, 2016
www.ann-geophys.net/34/1031/2016/
doi:10.5194/angeo-34-1031-2016

Annales Geophysicae Open Access EGU

Analysis of aerosol absorption properties and transport over North Africa and the Middle East using AERONET data

Ashraf Farahat[1,2], Hesham El-Askary[3,4,5], Peter Adetokunbo[6], and Abu-Tharr Fuad[7]

[1]Department of Prep Year Physics, College of Applied and Supporting Studies, King Fahd University of Petroleum & Minerals, Dhahran 31261, Saudi Arabia
[2]Department of Physics, Faculty of Science, Moharam Beek, Alexandria University, Alexandria, 21522, Egypt
[3]Center of Excellence in Earth Systems Modeling and Observations, Chapman University, Orange, CA 92866, USA
[4]Schmid College of Science and Technology, Chapman University, CA 92866, USA
[5]Department of Environmental Sciences, Faculty of Science, Moharam Beek, Alexandria University, Alexandria, 21522, Egypt
[6]Department of Geology, State University of New York at Buffalo, Buffalo, NY 14260, USA
[7]Department of Chemistry and Earth Science, College of Arts & Science, Qatar University, Doha, Qatar

Correspondence to: Hesham El-Askary (elaskary@chapman.edu)

Received: 22 July 2016 – Revised: 4 October 2016 – Accepted: 11 October 2016 – Published: 17 November 2016

Abstract. In this paper particle categorization and absorption properties were discussed to understand transport mechanisms at different geographic locations and possible radiative impacts on climate. The long-term Aerosol Robotic Network (AERONET) data set (1999–2015) is used to estimate aerosol optical depth (AOD), single scattering albedo (SSA), and the absorption Ångström exponent (α_{abs}) at eight locations in North Africa and the Middle East. Average variation in SSA is calculated at four wavelengths (440, 675, 870, and 1020 nm), and the relationship between aerosol absorption and physical properties is used to infer dominant aerosol types at different locations. It was found that seasonality and geographic location play a major role in identifying dominant aerosol types at each location. Analyzing aerosol characteristics among different sites using AERONET Version 2, Level 2.0 data retrievals and the Hybrid Single Particle Lagrangian Integrated Trajectory model (HYSPLIT) backward trajectories shows possible aerosol particle transport among different locations indicating the importance of understanding transport mechanisms in identifying aerosol sources.

Keywords. Atmospheric composition and structure (aerosols and particles; pollution – urban and regional)

1 Introduction

Natural and anthropogenic aerosols suspended in the atmosphere are characterized by their diverse sources, varying particle dynamics, lifetimes, interactive mechanisms, and surface and column distributions. Identifying mixtures containing multiple aerosol types like dust, carbon, sea salt, sulfate, or nitrogen is challenging for spaceborne and in situ observations (Chin et al., 2002; Farahat, 2016). Optical techniques are used to estimate particle sizes; however, determining particle types requires more information regarding aerosol sources, trajectories, regional topography, and atmospheric conditions. As for radiative impacts, aerosol characterization and types are major input parameters for obtaining precise climate predictions (Ramanathan et al., 1989; Satheesh and Moorthy, 2005; Farahat et al., 2015). For instance, particle absorption characteristics are used in assessing aerosol emission sources, types, and interaction phases (El-Askary et al., 2015). Aerosol categorization also helps identify dominant aerosol types over a certain geographic location, while climatology effects due to aerosols' spatial and temporal distribution is carried out by examining aerosol sizes along with their absorption characteristics using modeling, satellites, and ground-based measurements (El-Askary, 2006; Kaskaoutis et al., 2012; Aboel Fetouh et al., 2013; Vukovic et al., 2014; Sprigg et al., 2014). It is noteworthy that

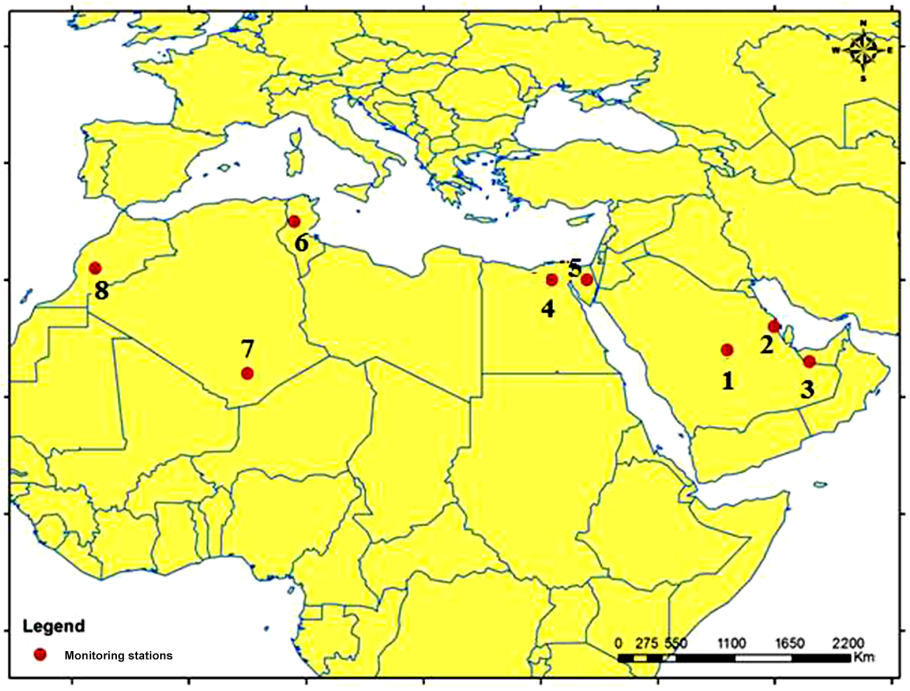

Figure 1. Location map of the AERONET stations used in this study with numbers on the map representing stations' locations: 1 – Solar Village; 2 – Bahrain; 3 – Mezaira; 4 – Cairo; 5 – Sedé Boqer; 6 – Ben Salem, 7 – Tamanrasset; and 8 – Saada.

aerosol optical and microphysical properties can provide significant information to categorize aerosol types. For example, parameters like aerosol optical depth (AOD), the Ångström exponent (AE), aerosol loading, and particle effective radius and different viewing angles are used to depict information regarding aerosol dominant types, emission sources, dust layers, and trajectories (Reid et al., 1999; Kaskaoutis and Kambezidis, 2006; Agarwal et al., 2007; Gobbi et al., 2007; Kalapureddy and Devara, 2008; Russell et al., 2010). Analyzing the derivatives of the AE and particle effective radius is also used to attain information regarding aerosol sizes and types since the particle types are directly correlated with sizes and optical properties (Gerasopoulos et al., 2003, 2011; Alados-Arboledas et al., 2003). The Aerosol Robotic Network (AERONET) data retrievals have been used widely to determine dominant aerosol types and categorization within mixing scenarios through investigating particle size distribution and optical and microphysical properties (Kaufman et al., 1994; Holben et al., 1998; Omar et al., 2005; Qin and Mitchell, 2009; Russell et al., 2010). These studies helped partition major aerosol types including dust, anthropogenic industrial pollution, and mixed and biomass burning aerosols. The absorption Ångström exponent (AAE), defined as the dependence of aerosol optical depth on wavelength as well as single scattering albedo (SSA), defined, as the ratio of scattering to extinction efficiency of aerosol particles, is used to categorize aerosol types. For instance, SSA for dust particles containing hematite and clay results in small absorption over the visible to near-infrared band and strong absorption around 440 nm (Sokolik and Toon, 1999). On the other hand, for organic carbon (OC), the SSA increases with increasing wavelength where the OC exhibits strong absorption in the visible and ultraviolet range, while for aerosols composed of black carbon (BC) particles, the SSA is inversely proportional to the wavelength. Sulfate and other hygroscopic aerosols do not show significant SSA spectral dependence (Dubovik et al., 2002). Therefore, mixed aerosol containing sulfates, BC, and OC could produce an indistinct SSA–wavelength dependence due to the varying spectral effects of aerosol mixtures in the atmosphere (Dubovik et al., 2002).

In this study we investigate aerosol characteristics over North Africa and the Middle East using eight AERONET sites in the region, namely, Solar Village (24° N, 46° E), Bahrain (26° N, 50° E), Mezaira (23° N, 53° E), Cairo (30° N, 31° E), Sedé Boqer (30° N, 34° E), Tamanrasset (22° N, 5° E), Saada (31° N, 8° W), and Ben Salem (35° N, 9° E) (Fig. 1). The analysis was based on data availability (at least 4 years of successive data measurements from 1999 to 2015) except for the Ben Salem site where the analysis was based on 2013–2015 data only. Previous studies (Table 1) classified dominant aerosol types at some of these sites based on their geographic locations into clear, dust, pollution, and mixed; however, the effect of seasonality and aerosol transport was not fully investigated for those sites. Dust and biomass particles could be dominating over some sites; however, other aerosol types could also exist over the

Table 1. Previous studies categorizing aerosol types over some of the AERONET sites presented in this work.

Aerosol type – region(s)	AERONET sites	References
Biomass – North Africa	Cairo	El-Askary and Kafatos (2008); Marey et al. (2010, 2011); El-Metwally et al. (2008)
Mixed – Middle East	Sedé Boqer	Derimian et al. (2006); Eck el. (2010)
Dust – Middle East	Solar Village, Bahrain, Mezaira	Dubovik and King (2000); Dubovik et al. (2002)
Different aerosol types	All Sites	Holben et al. (2001)
Mixed – North Africa	Saada, Tamanrasset, Ben Salem	Basart et al. (2009); Abdi Vishkaee et al. (2012)

site during the analysis period (Takemura et al., 2000; El-Askary and Kafatos, 2008). Although previous studies categorized sites based on their most dominant aerosol particles, they did not explicitly explore the variability in aerosol types over each site. As seasonal changes, major dust events, and human activities could largely affect dominant aerosol types (El-Metwally et al., 2008). Each location could have more than one dominating particle category during the year. In this work, we analyze aerosol volume size parameters and compare them with single scattering albedo at each site. The absorption parameters are calculated at various wavelengths. Last, aerosol variability and possible transport from one site to another is investigated. This study highlights this variability in aerosol categorization over each site based on these factors. It also shows possible aerosol transport between sites. The following criteria are used to categorize aerosol particles based on AOD (τa675) and the Ångström exponent (α675/440) (El-Askary et al., 2009). Cases with $\tau a675 \geq 0.3$ and $\alpha 675/440 \leq 0.4$ are classified as dust; $\tau a675 < 0.3$ and $\alpha 675/440 > 0.8$ are classified as pollution; $\tau a675 \geq 0.3$ and $\alpha 675/440 > 0.4$ are classified as mixed; $\tau a675 < 0.3$ are classified as clean.

2 Instrumentation, data, and methodology

AERONET is an array of sun photometers globally distributed to measure columnar spectral AOD and water vapor in a wavelength range of 340 to 1640 nm and temporal resolution of 600 to 900 s. The network also retrieves columnar optical aerosol properties (e.g., aerosol size distribution, volume mean radius, volume concentration, and multi wavelength single scattering albedo at 440, 675, 870, and 1020 nm (Holben et al., 1998)). This takes place by fitting measurements of the spectral AOD and sky radiances to radiative transfer calculations (Dubovik and King, 2000). AERONET data retrievals comprise 1–2 % estimated uncertainty (Eck et al., 1999) with the highest uncertainty near UV wavelengths (Holben et at., 1998). We used the AERONET Version 2, Level 2.0 products that contain retrievals for 116 different aerosol parameters including, aerosol volume size distribution (AVSD; $dV(r)/d\ln r$ ($\mu m^3/\mu m^2$)) retrieved in 22 logarithmically equidistant radial bins spanning the range of particle radii $0.05\,\mu m \leq r \leq 15\,\mu m$, the real and imaginary parts of the refractive index (CRI-R(λ), CRI-I(λ)), and the optical parameters (AOD (λ) and SSA) centered at four wavelengths (440, 675, 870, and 1020 nm; Taylor et al., 2014). Version 2 inversion products also provide the mean geometric radii of the fine and coarse modes, their standard deviation, and their volume concentrations. This is of particular importance for our analysis owing to the mixing scenarios observed over North Africa and the Gulf region.

The AERONET inversion code provides aerosol optical properties by measuring spectral direct beam and diffuse solar radiation. Water vapor and columnar spectral AOD characteristics can be retrieved from the AERONET direct-sun measurements with a temporal resolution of $\sim$ 600–900 s and 1–2 % typical AOD uncertainty (Holben et al., 1998; Eck et al., 1999). Depending on the site, the data are typically provided at a wavelength range of 340 to 1640 nm, together with Ångström exponent α over certain wavelength ranges. AERONET pre-version 1 (pre-release of Version 1, 2003) data have been applied to categorize aerosols based on their optical characteristics (Dubovic et al., 2002, and Russell et al., 2010). The AERONET Version 2 data, 2006, provided more precise calculations of reflectance over bright surfaces compared to Version 1. For example, in Saudi Arabia, Bahrain, and the United Arab Emirates, Version 2 provided more consistent SSA over small islands vs. vast bright desert, with an SSA difference of less than 0.01 compared to 0.03 for Version 1.

AERONET data retrievals Version 2, Level 2.0 (Smirnov et al., 2000, 2002) are used to derive the extinction Ångström exponent (α_{ext}) using the measured aerosol optical properties and AOD spectral dependence (τ_{ext}) with wavelength (λ)

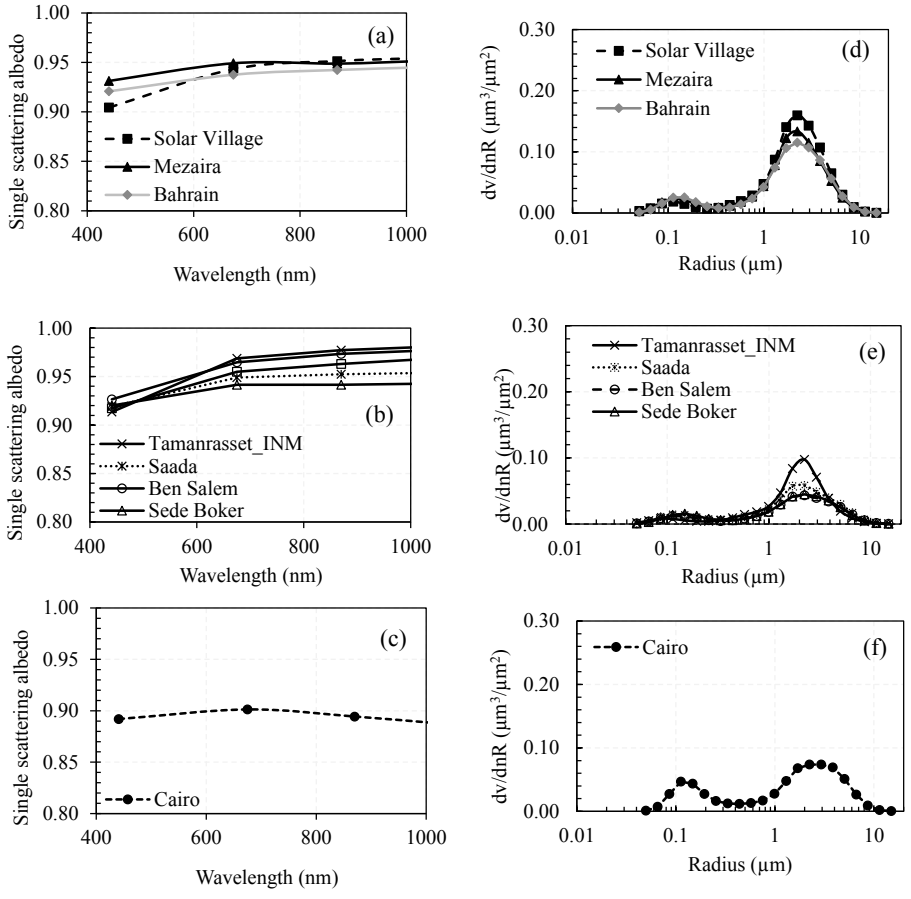

Figure 2. Characteristics of the single scattering albedo (SSA) at **(a)** Solar Village, Bahrain, and Mezaira; **(b)** Tamanrasset, Saada, Ben Salem, and Sedé Boqer; **(c)** Cairo. Volume size distribution at the eight sites: **(d)** Solar Village, Bahrain, and Mezaira; **(e)** Tamanrasset, Saada, Ben Salem, and Sedé Boqer; **(f)** Cairo.

(Ångström, 1964):

$$\alpha_{\text{ext}} = -\mathrm{d}\ln[\tau_{\text{ext}}(\lambda)]/\mathrm{d}\ln(\lambda). \quad (1)$$

Fine- and coarse-mode particles can be identified by calculating the linear regression of $\ln(\tau_{\text{ext}})$ vs. $\ln(\lambda)$, where values close to 2 indicate fine mode and 0 represents coarse mode (Nakajima et al., 1989). The absorption Ångström exponent (α_{abs}) can also be calculated using

$$\alpha_{\text{abs}} = -\mathrm{d}\ln[\tau_{\text{abs}}(\lambda)]/\mathrm{d}\ln(\lambda). \quad (2)$$

Aerosol particle physical characteristics affect α_{abs}, for example α_{abs} varies from less than 1.0 and up to 1.6 for large black carbon particles ($r > 0.1\,\mu\text{m}$) based on their core size and coating structure (Kondo et al., 2009). Black carbon particles are characterized by their small radius and spherical shapes, which results in α_{abs} values of ~ 1.0 (Petzold et al., 1997). Dubovik et al. (2002) also showed that α_{abs} varies between 1.2 and 3.0 for dust, 1.2 and 2.0 for pollution (biomass only), and 0.75 and 1.3 for mixed aerosols.

3 Results

3.1 Aerosol categorization using SSA

Aerosol absorption properties over the eight locations under investigation are represented in Fig. 2 and Table 2. The SSA spectral behavior agrees with Giles et al. (2012) and Dubovik et al. (2002) but with an average decrease of 0.02 at the Solar Village and Bahrain sites. The averaged optical properties, with aerosol data listed and volume size distribution at each site (Table 2), shows there is a lower SSA variability at Solar Village, Mezaira, and Bahrain compared to the other sites. The small SSA variability at those three sites is attributed to physical (size and shape) similarities between particle grains produced by the vast sand area surrounding the sites. The SSA standard deviations calculated for this study are 0.004 lower and 0.008 greater than Dubovik et al. (2002) for the Solar Village and Bahrain sites, respectively. The difference between Table 2 and Dubovik et al. (2002) for these two sites is due to applying improved Level 2.0 AERONET data retrievals and utilizing a larger data set. Pure dust could be dis-

Table 2. Aerosols absorption and physical properties categorized by aerosol types, for sample stations, using AERONET Version 2, Level 2.0 data retrievals. Some locations may experience other aerosol types during different seasons (Cairo, for instance). The spectral single scattering albedo (SSA) is listed first followed by the standard deviations based on monthly values. EMA: Egyptian Meteorology Authority.

Site	Data range	SSA 440/675/870/1020	α_{abs}	α_{ext}	N
		Dust			
Solar Village	1999–2015	0.9/0.94/0.95/0.95 0.0225/0.0261/0.0269/0.0276	1.5 ± 0.54	0.35 ± 0.13	4080
Bahrain	1996–2006	0.92/0.94/0.94/0.94 0.0296/0.0265/0.0280/0.0297	1.3 ± 0.47	0.58 ± 0.22	1320
Mezaira	2004–2015	0.93/0.95/0.95/0.95 0.0178/0.0181/0.0223/0.0243	1.2 ± 0.18	0.49 ± 0.44	1500
		Biomass			
Cairo EMA	2005–2007	0.89/0.90/0.90/0.90 0.0203/0.0234/0.0275/0.0306	1.2 ± 0.32	0.88 ± 0.44	360
Cairo Univ.	2004–2005	0.89/0.90/0.88/0.87 0.0140/0.0268/0.0357/0.0435	0.94 ± 0.31	0.83 ± 0.35	210
		Mixed			
Sedé Boqer	2010–2015	0.92/0.94/0.94/0.94 0.0240/0.0273/0.0345/0.0373	1.2 ± 0.27	0.72 ± 0.45	3180
Saada	2003–2015	0.92/0.95/0.95/0.95 0.0226/0.0206/0.0249/0.0279	1.3 ± 0.21	0.57 ± 0.48	1560
Ben Salem	2013–2015	0.93/0.96/0.97/0.98 0.0211/0.0129/0.0126/0.0129	1.9 ± 0.23	0.62 ± 0.71	420
Tamanrasset	2000–2015	0.91/0.97/0.98/0.98 0.0139/0.0072/0.0054/0.0049	2.1 ± 0.09	0.25 ± 0.76	540

tinguished for values of α_{ext} less than 0.2 (Kim et al., 2011). Solar Village, Bahrain, and Mezaira have $\alpha_{ext} \geq 0.3$, indicating a possible incursion by other aerosols. This is more recognized at the Bahrain site due to the presence of fine particles produced from industrial activities similar to other locations (Gathman, 1983; Gras, 1995; Kalapureddy and Devara, 2008; Park et al., 2015).

Cairo is known for its widespread biomass burning activities observed during fall when episodes of ash burning from agriculture waste take place (El-Askary and Kafatos, 2008; Marey et al., 2010, 2011); however, other factors could also contribute to pollution, such as traffic and industry. Compared to other particle types, the biomass particles are known to have the largest SSA variability due to various combustion phases and fuel types (Eck et al., 2003); however, only a small SSA difference (~ 0.013) is observed between Cairo and the Solar Village, Bahrain, and Mezaira site. This is an indication of a possible mixing pattern between biomass and dust over Cairo (El-Askary and Kafatos, 2008; El-Metwally et al., 2008).

The similarity in the SSA characteristics between the Saada, Tamanrasset, and Ben Salem sites, on the one hand, and Solar Village, Bahrain, and Mezaira (Fig. 2) with a strong absorption at 440 nm, on the other hand, is an indication of the dust dominance contribution to the Saada, Tamanrasset, and Ben Salem sites. The increased absorption at these three sites could also be due to increased hematite percentage in the dust that could lead to an increased absorption in the blue to near-infrared wavelength band (Sokolik and Toon. 1999). The average SSA values for all locations are ~ 0.91 (440 nm), 0.94 (675 nm), 0.95 (870 nm), and 0.95 (1020 nm) and reveal insignificant changes with respect to the SSA for all sites (Fig. 2, and Table 2). This is a sign of possible mixing scenarios through transporting aerosols between different sites.

Figure 2d–f show that both small and large particles exist with large particles dominating , as is shown by the two peaks at ~ 0.1 and ~ 4 µm with high dust domination over the Solar Village, Bahrain, and Mezaira locations. The high concentration of small size particles with ~ 0.1 µm over Cairo is an indication of high pollution over this location.

3.2 Aerosol (pollution/dust) discrimination using Ångström exponent

The AERONET Lev 2, Ver 2.0 data retrievals are used along with Eq. 2 to calculate average absorption aerosol optical depth (τ_{abs}) and the absorption Ångström exponent (α_{abs}) for aerosol particles at the Solar Village, Bahrain, and Mezaira (Fig. 3, Table 2). A comparison with Giles et al. (2012) shows a large difference in α_{abs} (+0.47), and with Dubovik

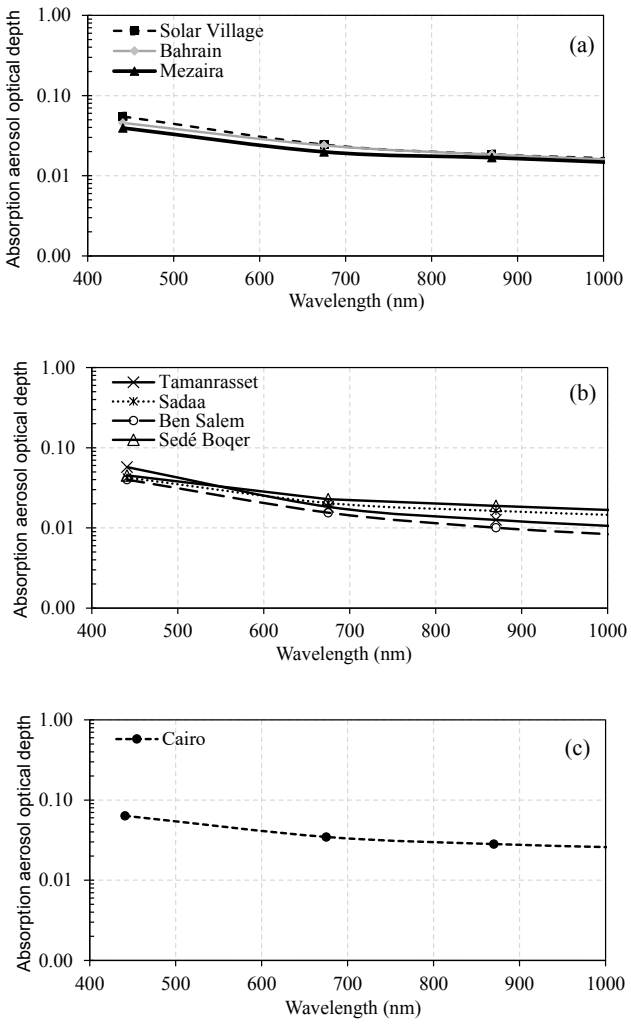

Figure 3. Absorption aerosol optical depth (τ_{abs}) average grouped by the dominant aerosol type at the eight sites using AERONET Version 2, Level 2.0 data retrievals: **(a)** Solar Village, Bahrain, and Mezaira; **(b)** Tamanrasset, Saada, Ben Salem, and Sedé Boqer; **(c)** Cairo.

et al. (2002), Giles et al. (2012), and Russell et al. (2010), the difference in α_{abs} over Solar Village is (+0.3). For the Tamanrasset, Saada, Ben Salem, Sedé Boqer, and Cairo sites, the average α_{abs} is comparable to Russell et al. (2010) and Giles et al. (2012).

The above results can give a general indication regarding aerosol categorizations at different locations and possible particle transport mechanism; however, they do not show the seasonality effect on particle dominance over a certain location. Long-range frequency of occurrence of clean, mixed, dust, and pollution aerosol categories along with their AOD and Ångström exponent measurements over the Solar Village, Bahrain, Mezaira, Sedé Boqer, Cairo, Saada, Tamanrasset, and Ben Salem stations can provide detailed information of the aerosol categorization and transport patterns

Table 3. Seasonal dust domination over study locations. EMA: Egyptian Meteorology Authority.

		Dust	
	Date	τa675	α675/440
Solar Village	Jun 2000	0.334636	0.123701
	Jul 2000	0.554335	0.209781
	May 2003	0.647241	0.089842
	Jun 2003	0.427258	0.259769
	May 2004	0.478263	0.135207
	May 2006	0.675854	0.136249
	Apr 2007	0.565676	0.216993
	May 2007	0.525404	0.229953
	Jun 2007	0.512271	0.222469
	May 2008	0.603597	0.219008
	Jun 2008	0.581412	0.136546
	Apr 2009	0.525053	0.160235
	May 2009	0.683702	0.154192
	Jun 2009	0.841581	0.180778
	Mar 2010	0.427101	0.230243
	May 2011	0.635264	0.156087
	May 2012	0.580928	0.220351
	Jun 2012	0.549905	0.34144
Bahrain	May 2006	0.451065	0.300185
Mezaira	May 2010	0.40083	0.363177
	Jun 2010	0.487617	0.372444
	Mar 2012	0.591211	0.306378
Cairo EMA	Apr 2005	0.440351	0.609703
Saada	Jul 2007	0.421629	0.392435
	Jul 2010	0.503962	0.312905
	Aug 2011	0.399346	0.387933

among sites. Tables 3–6 and Fig. 4a–c show the effect of seasonality in determining the dominant aerosol particles at each location. Table 3 shows that natural dust particles dominate over the Solar Village, Bahrain, and Mezaira sites during March–June where dust storms events are active during these months. Anthropogenic aerosols dominate over the sites mostly during September–December (Table 4) due to common windstorms (Said and Kadry, 1994) blowing during these months, which help in transporting pollutants and other anthropogenic aerosols. A mixed aerosol pattern is observed all year around over the three sites but mostly during July and August (Table 5), and the air is mostly clean during November and December (Table 6). AOD values and Ångström exponents played a major role in defining the abovementioned four aerosol categories represented in Tables 3–6.

Data showed that high pollution over Cairo during the autumn months (Table 4, Fig. 4e) as a result of yearly events where farmers burn their leftover rice straw, causing severe pollution and 2 to 3 months of potential complications for respiratory and heart disease patients (Marey et al., 2010). It is interesting to observe similar pollution patterns over

Table 4. Seasonal pollution domination over study locations.

		Pollution	
Solar Village	Sep 1999	0.244095	0.867438
	Oct 2002	0.183753	0.926034
	Oct 2004	0.167256	0.906812
	Nov 2005	0.191312	0.86848
	Dec 2006	0.196497	1.019745
	Oct 2007	0.175421	1.057346
	Nov 2007	0.129448	0.904911
	Dec 2007	0.176361	0.899631
	Dec 2009	0.172281	0.825395
	Dec 2010	0.13846	1.046825
	Oct 2012	0.202834	1.166223
	Dec 2012	0.217803	0.858837
Bahrain	Oct 2004	0.291991	1.081508
	Nov 2004	0.271147	1.07103
	Dec 2004	0.181128	1.298788
	Jan 2005	0.251857	0.984849
	Feb 2005	0.246111	0.881871
	Sep 2005	0.255824	0.852505
	Oct 2005	0.251038	1.219987
	Nov 2005	0.236496	1.125288
	Dec 2005	0.214268	1.20609
	Jan 2006	0.245147	1.04383
	Sep 2006	0.288577	0.890148
Mezaira	Sep 2007	0.254272	0.888841
	Oct 2007	0.202455	1.132523
	Dec 2007	0.13286	1.12398
	Oct 2008	0.238893	0.825587
	Nov 2008	0.145263	1.247883
	Nov 2009	0.162022	1.004461
	Dec 2009	0.168218	1.153539
	Jan 2010	0.122813	1.353932
	Nov 2010	0.176654	1.398123
	Sep 2011	0.294382	0.932607
	Oct 2011	0.219481	0.943015
	Nov 2013	0.154019	1.215744
	Dec 2013	0.119431	1.156596
	Jan 2014	0.147758	1.236338
Sedé Boqer	Aug 1998	0.174121	1.288291
	Sep 1998	0.166246	1.11584
	Jul 1999	0.132953	1.250256
	Aug 1999	0.136223	1.21218
	Sep 1999	0.147045	1.031709
	Aug 2000	0.158882	1.082329
	Jul 2001	0.137293	1.095682
	Aug 2001	0.177398	1.23571
Sedé Boqer	Jul 2003	0.107682	1.340217
	Nov 2003	0.128659	1.037325
	Jun 2004	0.112256	1.090375
	Jul 2004	0.124242	1.091038
	Aug 2004	0.107275	1.238889
	Sep 2004	0.129063	1.170213
	Oct 2004	0.188042	1.002594
	May 2005	0.160178	1.013421
	Jun 2005	0.162945	1.061923
	Jul 2005	0.117386	1.30013
	Aug 2005	0.141749	1.235765
	Sep 2005	0.135074	1.098233
	Oct 2005	0.130501	1.167848
	Nov 2005	0.095973	1.33766
	Jul 2006	0.130309	1.324776
	Aug 2006	0.137575	1.143954
	Sep 2006	0.147521	1.107143
	Oct 2006	0.126813	1.211563
	Nov 2006	0.091998	1.324415
	Jan 2007	0.090471	1.242201
	Jul 2007	0.124851	1.234827
	Aug 2007	0.124037	1.25921
	Dec 2007	0.069032	1.245291
	Jul 2008	0.099229	1.211103
	Aug 2008	0.177886	1.259835
	Oct 2008	0.1479	1.201744
	Nov 2008	0.085567	1.351784
	Dec 2008	0.069011	1.247196
	Jun 2009	0.109275	1.033012
	Jul 2009	0.118304	1.176056
	Aug 2009	0.113501	1.401656
	Sep 2009	0.120057	1.335245
	Oct 2009	0.194083	1.044277
	Nov 2009	0.094559	1.457584
	Dec 2009	0.101495	1.294266
	Jan 2010	0.090991	1.131905
	Jul 2010	0.17596	1.051998
	Aug 2010	0.191311	1.034425
	Nov 2010	0.12169	1.095045
	Mar 2011	0.118081	1.0387
	Jun 2011	0.116627	1.305029
	Jul 2011	0.158914	1.298425
	Aug 2011	0.121009	1.387253
	Sep 2011	0.131061	1.463028
	Oct 2011	0.141843	1.098022
	Nov 2011	0.096901	1.433644

Sedé Boqer (Fig. 4c) during the same time of the year indicating a possible aerosol transport between different sites. Data show that dust particles dominate over Cairo during the spring season with the yearly khamsin sandstorm blowing over the country during this time. These results agree with a high fine-particle concentration found over Cairo (Fig. 2f).

Dust particles dominate over the Saada site (Table 3, Fig. 4f) during July and August, which is not the usual sand storm season (February–April) over Morocco (Goudie and Middleton, 2001). However, this could be attributed to the effect of single dust events sweeping off the coast of Morocco, like the ones on 15 August 2005 and on 7 August 2015.

Table 4. Continued.

		Pollution	
Sedé Boqer	Jun 2012	0.137811	1.050994
	Jul 2012	0.123867	1.300216
	Aug 2012	0.104786	1.323267
	Sep 2012	0.14309	1.177
	Oct 2012	0.143002	1.305639
	Nov 2012	0.111837	1.22663
	Dec 2012	0.075735	1.083349
	Jun 2013	0.140469	1.004892
	Jul 2013	0.097441	1.305687
	Aug 2013	0.094034	1.352441
	Jul 2014	0.10121	1.384998
	Aug 2014	0.096176	1.409582
	Sep 2014	0.122792	1.139754
	Oct 2014	0.1075	1.349438
	Nov 2014	0.078158	1.212458
Cairo Univ.	Nov 2004	0.214229	1.175515
	Dec 2004	0.202082	1.291856
	Jan 2005	0.228575	1.118635
	Mar 2005	0.219945	1.223339
Cairo EMA	May 2005	0.247344	1.063784
	Jun 2005	0.288959	1.109003
	Jul 2005	0.255777	1.319079
	Aug 2005	0.261915	1.294556
	Sep 2005	0.26998	1.118464
	Nov 2005	0.234297	1.300921
	Dec 2005	0.251722	1.23849
	Jan 2006	0.231234	1.349487
Tamanrasset	Jan 2013	0.022714	1.100667
Saada	May 2007	0.129623	1.039977
	Nov 2007	0.118411	1.024152
	Dec 2007	0.072318	1.45022
	Jan 2008	0.062712	1.449272
	May 2008	0.132574	1.080527
	Dec 2011	0.082039	1.267306
	Feb 2012	0.10336	1.119926
Ben Salem	Aug 2013	0.177932	1.042051
	Apr 2014	0.114515	1.000073

Tamanrasset site data indicate that dust dominates (Fig. 4g) during March–April, which falls within the yearly dust storm events over Algeria and in October–November where individual dust events blow through the Sahara. Clear weather conditions are also found all year around. The Ben Salem (Fig. 4h) station does not provide enough data during the study period but most of the data collected point to a mixing aerosol particle pattern during May–July. Time series of the AOD and Ångström exponent show a data gap over the Mezaira, Cairo, Saada, and Ben Salem stations where the sun photometers were not operating for an extended period.

Table 5. Seasonal mixing particle domination over study locations.

		Mixed	
Solar Village	May 1999	0.341644	0.426579
	Aug 2000	0.398135	0.634875
	Jul 2003	0.317711	0.510211
	Aug 2003	0.359311	0.60482
	Jul 2005	0.359354	0.441735
	Aug 2005	0.303309	0.559758
	Jul 2006	0.31427	0.411585
	Aug 2006	0.420226	0.519463
	Sep 2007	0.304047	0.745258
	Aug 2009	0.504137	0.400734
	Sep 2009	0.353579	0.482951
	Feb 2011	0.390127	0.418135
	Jun 2011	0.607849	0.409912
	Jul 2011	0.49618	0.573132
	Aug 2011	0.37496	0.639556
	Jul 2012	0.383708	0.739601
	Aug 2012	0.328888	0.81767
Bahrain	Mar 2005	0.309838	0.642457
	Apr 2005	0.409481	0.472898
	May 2005	0.510207	0.479964
	Jun 2005	0.379552	0.40134
	Jul 2005	0.50564	0.543538
	Aug 2005	0.396494	0.794101
	Feb 2006	0.316549	0.725944
	Mar 2006	0.339703	0.452933
	Apr 2006	0.441408	0.494285
	Jun 2006	0.345064	0.728788
	Jul 2006	0.380813	0.702739
	Aug 2006	0.51552	0.860817
Mezaira	Jul 2004	0.36782	0.536964
	Aug 2004	0.38091	0.617358
	Sep 2004	0.328915	0.526263
	Mar 2010	0.314758	0.453755
	May 2014	0.367042	0.634481
Sedé Boqer	May 2003	0.331628	0.454896
Cairo EMA	Apr 2005	0.440351	0.609703
Saada	Jul 2004	0.348132	0.455605
	Aug 2005	0.312071	0.566701
	May 2006	0.327604	0.669969
	Aug 2007	0.335435	0.66549
	Jul 2011	0.321371	0.599259
Ben Salem	May 2013	0.176807	0.776106
	Jun 2013	0.155888	0.796066
	Sep 2013	0.210805	0.755659
	May 2014	0.193105	0.761131
	Jul 2014	0.249383	0.701042

Over the Solar Village, large dust events were recorded during March–July with peak AOD observed in June 2009 (0.84), May 2009 (0.68), May 2006 (0.67), May 2003 (0.65), May 2011 (0,63), and March 2012 (0.59). It is clear that

Table 6. Seasonal clear events over study locations.

		Clean	
Solar Village	Nov 1999	0.149764	0.550323
	Jan 2003	0.096228	0.62666
	Oct 2003	0.178413	0.733404
	Mar 2004	0.191491	0.655569
	Oct 2005	0.18837	0.779462
	Nov 2005	0.191312	0.86848
	Oct 2006	0.180977	0.694947
	Dec 2007	0.176361	0.899631
	Dec 2009	0.172281	0.825395
	Jan 2010	0.124348	0.712725
Mezaira	Sep 2013	0.281399	0.792686
Sedé Boqer	May 2000	0.159897	0.605992
	Mar 2006	0.184774	0.75678
	Jun 2006	0.173092	0.765389
	Oct 2010	0.183684	0.67544
	Mar 2013	0.182458	0.506042
	Apr 2014	0.149829	0.625146
	May 2014	0.162358	0.72418
	Jun 2014	0.188386	0.799814
Tamanrasset	Oct 2006	0.150022	0.312346
	Nov 2006	0.058332	0.711289
	Feb 2007	0.07994	0.543037
	Mar 2007	0.277462	0.350458
	Apr 2007	0.26391	0.250456
	Sep 2007	0.256329	0.490798
	Oct 2007	0.123111	0.613251
	Aug 2008	0.262444	0.5155
	Oct 2008	0.259001	0.270847
	Nov 2008	0.090616	0.532111
	Dec 2008	0.058681	0.712297
	Jan 2009	0.061793	0.572664
	Dec 2012	0.055298	0.74645
	Feb 2013	0.055164	0.714122
	Mar 2013	0.110328	0.509167
	Jul 2013	0.284419	0.319017
	Sep 2013	0.234119	0.209053
	Oct 2013	0.073054	0.571297
	Nov 2013	0.051243	0.623209

March is the month with the most frequent dust activity as major dust storms frequently blow during this time of the year. This would also indicate a higher probability of dust transportation within Saudi Arabia and the Arabian Peninsula during March. The major dust event that took place in March 2009 over Saudi Arabia could have contributed to the high AOD observed during this period, with a widespread heavy atmospheric dust load which was reported in Alharbi et al. (2013) and Farahat et al. (2016), who also suggested that the major plume of the March 2009 dust outbreak originated from several dust source areas extending across two regions – the Qasīm region lying some 500 km northwest of Riyadh within an active dust source region (Alharbi, 2009) and the Ad Dibdibah and Aş Şummān Plateau region, which is a major source of frequent dust storms in Saudi Arabia. Parts of it are in Iraq, and the south of Kuwait covers the northeastern part of the Ad Dahnā Desert. Alharbi et al. (2013) and Farahat et al. (2016) also reported that this storm was associated with an increase in AOD, wind speed, and a reduction in temperature and visibility, for few days following the storm. Similar AOD pattern was observed over the Bahrain and Mezaira stations with peak AOD observed in March 2012 (0.59) and June 2010 (0.49) over Mezaira and in May 2006 (0.45) over Bahrain. It is important to mention that the Bahrain station did not produce any data after October 2006.

Based on the available data, dust dominates over Cairo during March and April, which is coincident with khamsin storms, in which major dust plumes are transported from the Sahara to eastern Europe. It is clear that most of the year pollution episodes took place over Cairo with peak pollution during November–January with another peak (α_{ext}) observed in January 2006 (1.35), November 2005 (1.30), and December 2004 (1.29). This could be attributed to the activity of Egyptian farmers burning rice straw and other agricultural waste during this time of the year. As a result pollution events during these months could be contributing to direct and indirect radiative forcing by anthropogenic aerosols. These results agree with El-Askary et al. (2009) where peaks of biomass burning were found to occur in September (2001 and 2002) and in October (2003 and 2004) over the greater Nile Delta region as observed from the MODIS Terra satellite. El-Askary et al. (2009) also indicated that the long-range pollution observed over Cairo could be attributed to transport from southeast Europe.

Pollution dominates over the Solar Village, Bahrain, and Mezaira sites from October to December with α_{ext} during October 2012 (1.12), October 2007 (1.06), December 2010 (1.04), and December 2006 (1.02) over the Solar Village; December 2004 (1.29), October 2005 (1.22), December (1.21), and November 2005 over Bahrain; and November 2010 (1.39), January 2010 (1.35), November 2008 (1.25), and January 2014 (1.24) over Mezaira. Pollution over the three sites is in general attributed to a boom in the oil industry accompanied by large infrastructure requirements, the establishment of major cement industry in the area, an unprecedented high economic growth rate, low energy costs subsidized by the government, and a population increase. These all contribute to Saudi Arabia, Bahrain, and UAE environmental pollution (Farahat, 2016). Winter pollution dominates from October to December due to a reduction in dust blowing events over these months, which is an indicator of less pollution transport during that period. Clean scenarios are observed over the Solar Village, Bahrain, and Mezaira mostly during the summer season; this is probably due to less traffic pollution as schools are off and many locals travel to cooler places to escape high summer temperatures in this

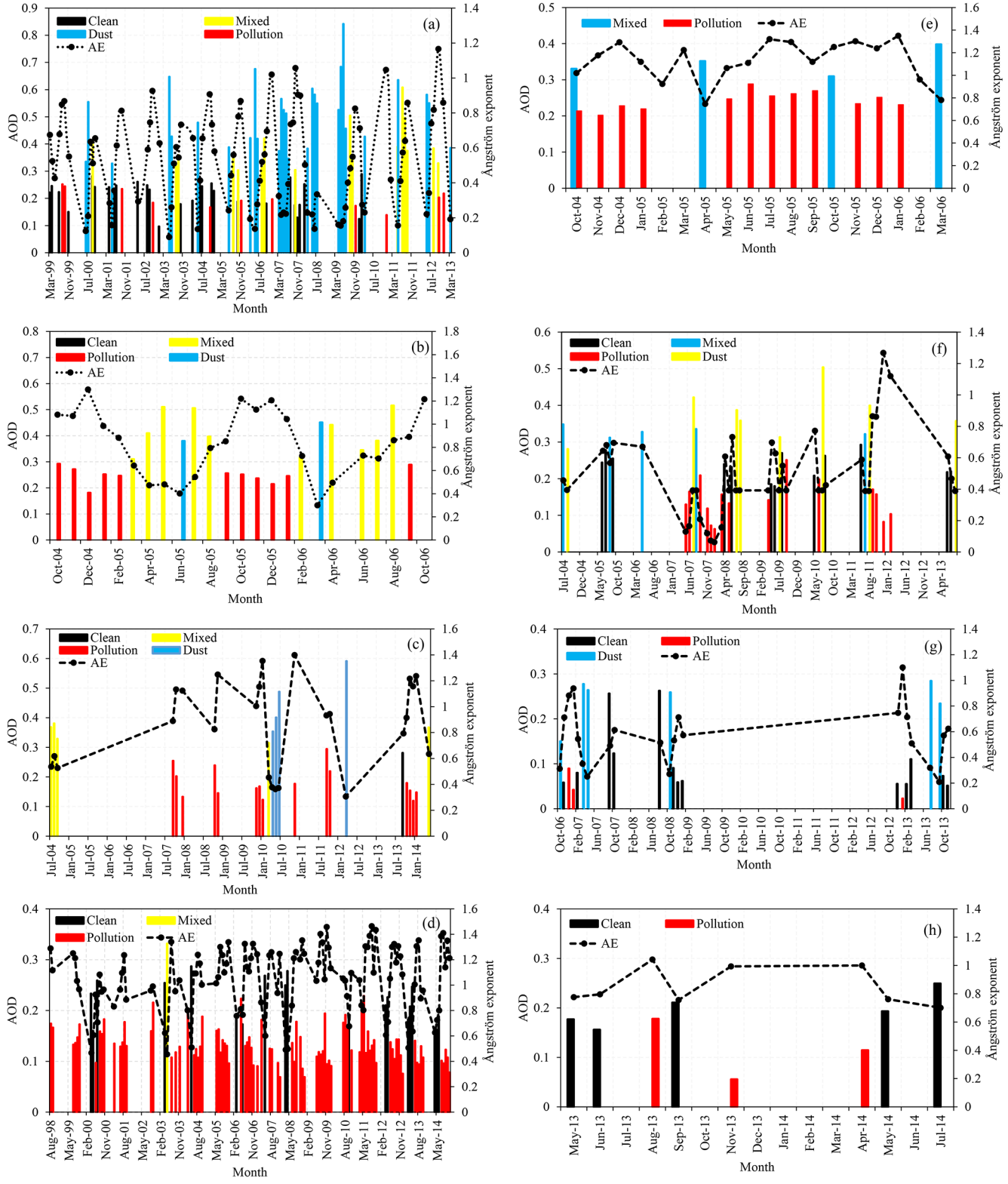

Figure 4. Measurements and occurrence for different aerosol particle categories and their corresponding absorption Ångström exponents (monthly average) over **(a)** Solar Village; **(b)** Bahrain; **(c)** Mezaira; **(d)** Sedé Boqer; **(e)** Cairo; **(f)** Saada; **(g)** Tamanrasset; **(h)** Ben Salem.

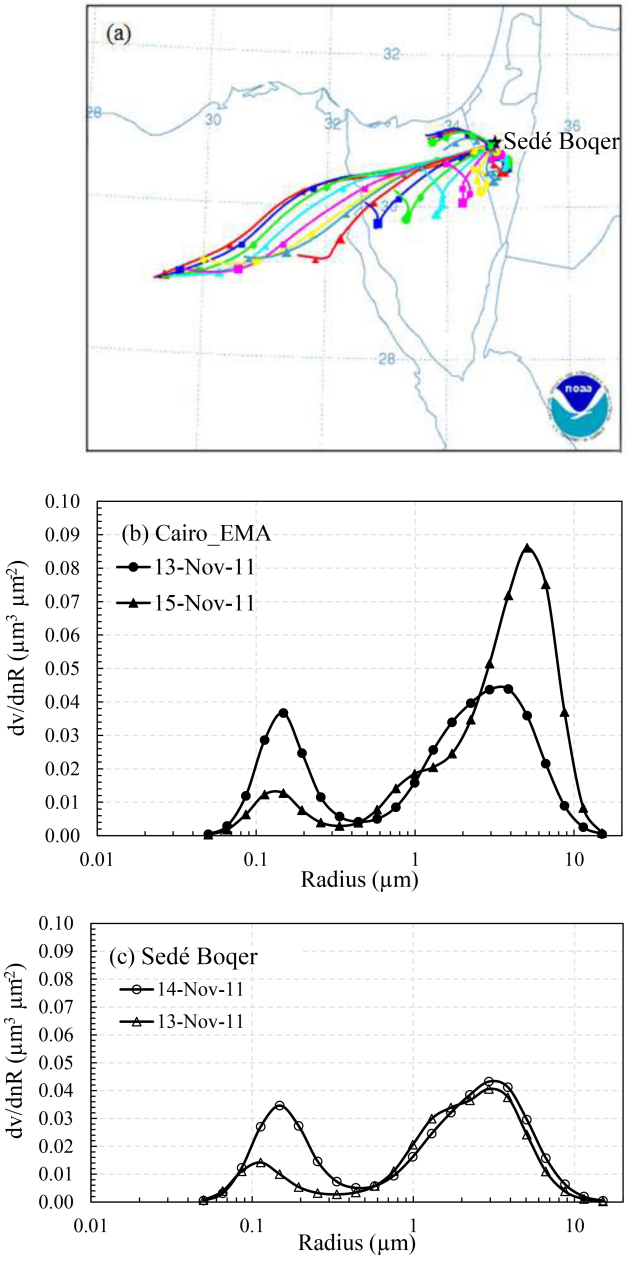

Figure 5. (a) HYSPLIT backward trajectory on 14 November 2011 at Sedé Boqer site showing aerosol possible transport from Cairo site; **(b)** volume size distribution at Sedé Boqer site during 13 and 14 November 2011; **(c)** volume size distribution at Cairo_EMA site during 13 and 15 November 2011.

area. However, clean weather is also observed during other months based on weather conditions and aerosol transport.

Compared to the Solar Village, Bahrain, and Mezaira sites, lower AOD values are recorded at the Tamanrasset and Saada sites during the dust season, but higher pollution is observed during November–February with α_{ext} January 2013 (1.10) over Tamanrasset; December 2007 (1.45), January 2008 (1.45), and December 2011 (1.26) over Saada; and August 2013 (1.04) over Ben Salem. Microparticle transport plays a major factor in changing aerosol types at different AERONET sites. In this article, we try to shed light on a possible aerosol transport between two AERONET sites, namely Cairo and Sedé Boqer. The two sites are chosen based on their geographic locations to demonstrate aerosol transport from North Africa to the Middle East. Aerosols volume size distribution on 13 November 2011 over the Cairo site and on 14 November 2011 over the Sedé Boqer site (24 h later) clearly shows aerosol transport between the two sites (Fig. 5). The Hybrid Single Particle Lagrangian Integrated Trajectory (HYSPLIT) back trajectory model confirms the possible aerosol transport from Cairo to Sedé Boqer. Gridded meteorological data, at regular time intervals, are used in the calculation of air mass trajectories. For the back-trajectories, data are obtained from existing archives. A complete description of input data, methodology, equations involved, and sources of error for the calculation of the air mass trajectory is presented by Draxler and Hess (1997). Figure 5a shows the air mass back trajectory at Sedé Boqer during the black cloud local pollution episode over the Delta Region at different vertical elevations to highlight the vertical extent of local transportation (Aboel Fetouh et al., 2013; Prasad et al., 2010). El-Askary and Kafatos (2008) found that an inversion layer contributes to the trapping of aerosols and pollutants, resulting in an increase of their concentration and, hence, creating a permanent haze that can develop into a health hazard. Figure 5b and c show the SSA characteristics over both locations, implying the transport from Cairo location to Sedé Boqer. SSA values at the finer radius size were high on the 13th over Cairo and low over Sedé Boqer; then SSA values increased on the 14th over Sedé Boqer while showing a drop on the 15th over Cairo. This behavior suggests aerosol transport from Cairo to Sedé Boqer during the period under investigation. The preliminary results here demonstrate a possible aerosol transport between different sites; however, a complete spatial and temporal analysis is needed to understand the effect of this transport on aerosol types.

4 Conclusions

A combination of ground-based aerosol-related parameters was used in this analysis to study different sources of aerosol loadings over eight different cities in North Africa and the Gulf region. Our analysis involved a study of the AOD and SSA, as well as other derived parameters and trajectory models. Natural vs. anthropogenic aerosols are well distinguished using our derived Ångström exponent. We also identified possible mixed and clean atmospheric conditions using the calculated α675/440 values. It is clear that dust episodes dominate the spring season, as reflected by the high values of AOD associated with sharp drops in the Ångström exponent. Back trajectory analysis shows agreement with these findings, thereby confirming that the Sahara is the major source

of such aerosols during the spring season. Furthermore, the sharp peaks in the Ångström exponent at the Cairo station suggests a possible long-range transport of pollutants from Europe during the summer season as previously discussed by El-Askary et al. (2009). Local pollution is most prominent during the fall and winter seasons, as confirmed by the data presented in the tables and associated figures. In summary, it is clear that the region under investigation is exposed to the impacts of aerosols from various sources throughout the year. This is becoming a serious health hazard because of the persistence of high pollution throughout the year or for prolonged time periods.

5 Data availability

All data used in this study are publicly available at the Aerosol Robotic Network (AERONET, 2016) homepage: http://aeronet.gsfc.nasa.gov/.

Acknowledgements. The authors would like to acknowledge the support provided by the Deanship of Scientific Research (DSR) at the King Fahd University of Petroleum and Minerals (KFUPM) for funding this work through project no. IN121064. The authors would like to also extend their thanks and appreciation to the principle investigators and their staff for establishing and maintaining the different AERONET sites (http://aeronet.gsfc.nasa.gov/) used in this investigation.

The topical editor, M. Salzmann, thanks three anonymous referees for help in evaluating this paper.

References

Abdi Vishkaee, F., Flamant, C., Cuesta, J., Oolman, L., Flamant, P., and Khalesifard, H.: Dust transport over Iraq and northwest Iran associated with winter shamal: a case study, J. Geophys. Res., 117, D03201, doi:10.1029/2011JD016339, 2012

Aboel Fetouh, Y., El-Askary, H., El Raey, M., Allali, M., Sprigg, W. A., and Kafatos, M.: Annual Patterns of Atmospheric Pollutions and Episodes over Cairo Egypt. Advances in Meteorology, 2013, 984853, doi:10.1155/2013/984853, 2013.

AERONET: Aerosol Characteristics, available at: http://aeronet.gsfc.nasa.gov/, last access: 15 November 2016.

Agarwal, A., El-Askary, H., El-Ghazawi, T., Kafatos, M., and Le-Moigne, J.: Efficient PCA Fusion Techniques for MISR Multi-angle Observations with Applications to Monitoring Dust Storms. IEEE Geosci. Remote S., 4, 678–682, doi:10.1109/LGRS.2007.904467, 2007.

Alharbi, B., Maghrabi, A., and Tapper N.: The March 2009 Dust Event in Saudi Arabia: Precursor and Supportive Environment, B. Am. Meteorol. Soc., 94, 515–528, 2013.

Alados-Arboledas, L., Lyamani, H., and Olmo, F. J.: Aerosol size properties at Armilla, Granada (Spain), Q. J. Roy. Meteor. Soc., 129, 1395–1413, 2003.

Alharbi, B. H.: Airborne dust in Saudi Arabia: Source areas, entrainment, simulation and composition. Ph.D. dissertation, Monash University, 313 pp., and Moied, K., 2005: Riyadh air quality report (1999–2004), King Abdulaziz City for Science and Technology 279-25-ER, 116 pp., 2009.

Ångström, A.: The parameters of atmospheric turbidity, Tellus A, 16, 64–75, 1964.

Basart, S., Pérez, C., Cuevas, E., Baldasano, J. M., and Gobbi, G. P.: Aerosol characterization in Northern Africa, Northeastern Atlantic, Mediterranean Basin and Middle East from direct-sun AERONET observations, Atmos. Chem. Phys., 9, 8265–8282, doi:10.5194/acp-9-8265-2009, 2009.

Chin, M., Ginoux, P., Kinne, S., Torres, O., Holben, B., Duncan, B., Martin, R., Logan, J., Higurashi, A., and Nakajima, T.: Tropospheric aerosol optical thickness from the GOCART model and comparisons with satellite and Sun photometer measurements, J. Atmos. Sci., 59, 461–483, 2002.

Derimian, Y., Karnieli, A., Kaufman, Y. J., Andreae, M. O., Andreae, T. W., Dubovik, O., Maenhaut, W., Koren, I., and Holben, B. N.: Dust and pollution aerosols over the Negev desert, Israel: Properties, transport, and radiative effect, J. Geophys. Res., 111, D05205, doi:10.1029/2005JD006549, 2006.

Draxler, R. R. and Hess, G. D.: Description of the HYSPLIT_4 modeling system, NOAA, Technical Memorandum ERL ARL-224, 24 pp., 1997.

Dubovik, O. and King, M. D.: A flexible inversion algorithm for retrieval of aerosol optical properties from Sun and sky radiance measurements, J. Geophys. Res., 105, 20673–20696, 2000.

Dubovik, O., Holben, B., Eck, T., Smirnov, A., Kaufman, Y., King, M., Tanre, D., and Slutsker, I.: Variability of absorption and optical properties of key aerosol types observed in worldwide locations, J. Atmos. Sci., 59, 590–608, 2002.

Eck, T., Holben, B., Reid, J., Dubovik, O., Smirnov, A., O'Neill, N., Slutsker, I., and Kinne, S.: Wavelength dependence of the optical depth of biomass burning, urban, and desert dust aerosols, J. Geophys. Res., 104, 31333–31349, 1999.

Eck, T., Holben, B., Reid, J., O'Neill, N., Schafer, J., Dubovik, O., Smirnov, A., Yamasoe, M., and Artaxo, P.: High aerosol optical depth biomass burning events: A comparison of optical properties for different source regions, Geophys. Res. Lett., 30, 2035, doi:10.1029/2003GL017861, 2003.

Eck, T. F., Holben, B. N., Sinyuk, A., Pinker, R. T., Goloub, P.,Chen, H., Chatenet, B., Li, Z., Singh, R. P., Tripathi, S. N., Reid, J. S., Giles, D. M., Dubovik, O., O'Neill, N. T., Smirnov, A., Wang, P., and Xia X.: Climatological aspects of the optical prop-erties of fine/coarse mode aerosol mixtures, J. Geophys. Res., 115, D19205, doi:10.1029/2010JD014002, 2010

El-Askary, H.: Air pollution Impact on Aerosol Variability over mega cities using Remote Sensing Technology: Case study, Cairo, The Egyptian Journal of Remote Sensing and Space Sciences, 9, 31–40, 2006.

El-Askary, H. and Kafatos, M.: Dust Storm and Black Cloud Influence on Aerosol Optical Properties over Cairo and the Greater Delta Region, Egypt, Int. J. Remote Sens., 29, 7199–7211, 2008.

El-Askary, H., Farouk, R., Ichoku, C., and Kafatos, M.: Transport of dust and anthropogenic aerosols across Alexandria, Egypt, Ann. Geophys., 27, 2869–2879, doi:10.5194/angeo-27-2869-2009, 2009.

El-Askary, H., Park, S. K., Ahn, M. H., Prasad, A., and Kafatos, M.: On the detection and monitoring of the transport of an Asian

dust storm approaching the Korean Peninsula, J. Environ. Inf. 25, 99–116, 2015.

El-Metwally, M., Alfaro, S. C., AbdelWahab, M., and Chatenet, B.: Aerosol characteristics over urban Cairo: Seasonal variations as retrieved from Sun photometer measurements, J. Geophys. Res., 113, D14219, doi:10.1029/2008JD009834, 2008.

Farahat, A.: Air Pollution in Arabian Peninsula (Saudi Arabia, United Arab Emirates, Kuwait, Qatar, Bahrain, and Oman): Causes, Effects and Aerosol Categorization, Arab J. Geosci., 9, 196, doi:10.1007/s12517-015-2203-y, 2016.

Farahat, A., El-Askary, H., and Al-Shaibani, A.: Study of Aerosols' Characteristics and Dynamics over the Kingdom of Saudi Arabia using a Multi Sensor Approach Combined with Ground Observations, Advances in Meteorology, 2015, 247531, doi:10.1155/2015/247531, 2015.

Farahat, A., El-Askary, H., and Dogan, U.: Aerosols size distribution characteristics and role of precipitation during dust storm formation over Saudi Arabia, Aerosol Air Qual. Res., in press, 2016.

Gathman, S. G.: Optical properties of the marine aerosol as predicted by the Navy aerosol model, Opt. Eng., 22, 57–62, 1983.

Gerasopoulos, E., Amiridis, V., Kazadzis, S., Kokkalis, P., Eleftheratos, K., Andreae, M. O., Andreae, T. W., El-Askary, H., and Zerefos, C. S.: Three-year ground based measurements of aerosol optical depth over the Eastern Mediterranean: the urban environment of Athens, Atmos. Chem. Phys., 11, 2145–2159, doi:10.5194/acp-11-2145-2011, 2011.

Gerasopoulos, E., Andreae, M. O., Zerefos, C. S., Andreae, T. W., Balis, D., Formenti, P., Merlet, P., Amiridis, V., and Papastefanou, C.: Climatological aspects of aerosol optical properties in Northern Greece, Atmos. Chem. Phys., 3, 2025–2041, doi:10.5194/acp-3-2025-2003, 2003.

Giles, D. M., Holben, B. N., Eck, T. F., Sinyuk, A., Smirnov, A., Slutsker, I., Dickerson, R. R., Thompson, A. M., and Schafer, J. S.: An analysis of AERONET aerosol absorption properties and classifications representative of aerosol source regions, J. Geophys. Res., 117, D17203, doi:10.1029/2012JD018127, 2012.

Gobbi, G. P., Kaufman, Y. J., Koren, I., and Eck, T. F.: Classification of aerosol properties derived from AERONET direct sun data, Atmos. Chem. Phys., 7, 453–458, doi:10.5194/acp-7-453-2007, 2007.

Goudie, A. S. and Middleton, N. J.: Saharan dust storms: nature and consequences, Earth-Sci. Rev., 56, 179–204, 2011.

Gras, J. L.: CN, CNN and particle size in Southern Ocean air at Cape Grim, Atmos. Res., 35, 233–251, 1995.

Holben, B. N., Eck, T. F., Slutsker, I., Tanré, D., Buis, J. P., Setzer, A., Vermote, E., Reagan, J. A., Kaufman, Y. J., Nakajima, T., Lavenu, F., Jankowiak, I., and Smirnov, A.: AERONET: A federated instrument network and data archive for aerosol characterization, Remote Sens. Environ., 66, 1–16, 1998.

Holben, B., Tanré, D., Smirnov, A., Eck, T., Slutsker,I., Abuhassan, N., Newcomb, W., Schafer, J., Chatenet, B., Lavenu, F., Kaufman, Y., Vande Castle, J., Setzer, A., Markham, B., Clark, D., Frouin, R., Halthore, R., Karneli, A., O'Neill, N., Pietras, C., Pinker, R., Voss, K, and Zibordi, G.: An emerging ground-based aerosol climatology: Aerosol optical depth from AERONET, J. Geophys. Res., 106, 12067–12097, doi:10.1029/2001JD900014, 2001.

Kalapureddy, M. C. R. and Devara, P. C. S.: Characterization of aerosols over oceanic regions around India during pre-monsoon 2006, Atmos. Environ., 42, 6816–6827, 2008.

Kaskaoutis, D. G. and Kambezidis, H. D.: Investigation on the wavelength dependence of the aerosol optical depth in the Athens area, Q. J. Roy. Meteor. Soc., 132, 2217–2234, 2006.

Kaskaoutis, D. G., Prasad, A. K., Kosmopoulos, P. G., Sinha, P. R., Kharol, S. K., Gupta, P., El-Askary, H. M., and Kafatos, M.: Synergistic use of remote sensing and modeling for tracing dust storms in the Mediterranean, Advances in Meteorology, 2012, 861026, doi:10.1155/2012/861026, 2012.

Kaufman, Y. J., Gitelson, A., Karnieli, A., Ganor, E., Fraser, R. S., Nakajima, T., Mattoo, S., and Holben, B. N.: Size distribution and scattering phase function of aerosol particles retrieved from sky brightness measurements, J. Geophys. Res., 99, 10341–10356, 1994.

Kim, D., Chin, M., Yu, H., Eck, T. F., Sinyuk, A., Smirnov, A., and Holben, B. N.: Dust optical properties over North Africa and Arabian Peninsula derived from the AERONET dataset, Atmos. Chem. Phys., 11, 10733–10741, doi:10.5194/acp-11-10733-2011, 2011.

Kondo, Y., Sahu, L., Kuwata, M., Miyazaki, Y., Takegawa, N., Moteki, N., Imaru, J., Han, N. S., Nakayama, T., Kim-Oanh, N. T., Hu, M., Kim, Y. J., and Kita, K.: Stabilization of the Mass Absorption Cross Section of Black Carbon for Filter-Based Absorption Photometry by the Use of a Heated Inlet, Aerosol. Sci. Tech., 43, 741–756, 2009.

Marey, H. S., Gille, J. C., El-Askary, H. M., Shalaby, E. A., and El-Raey, M. E.: Study of the formation of the "black cloud" and its dynamics over Cairo, Egypt, using MODIS and MISR sensors, J. Geophys. Res., 115, D21206, doi:10.1029/2010JD014384, 2010.

Marey, H. S., Gille, J. C., El-Askary, H. M., Shalaby, E. A., and El-Raey, M. E.: Aerosol climatology over Nile Delta based on MODIS, MISR and OMI satellite data, Atmos. Chem. Phys., 11, 10637–10648, doi:10.5194/acp-11-10637-2011, 2011.

Nakajima, T., Tanaka, M., Yamano, M., Shiobara, M., Arao, K., and Nakanishi Y.: Aerosol optical characteristics in the yellow sand events observed in May, 1982 in Nagasaki, J. Meteorol. Soc. Jpn., 67, 279–291, 1989.

Omar, A. H., Won, J., Winker, D., Yoon, S., Dubovik, O., and McCormick, P.: Development of global aerosol models using cluster analysis of Aerosol Robotic Network (AERONET) measurements, J. Geophys. Res., 110, D10S14, doi:10.1029/2004JD004874, 2005.

Park, S., El-Askary, H., Sabbah, I., Kwak, H., Prasad, A., Lee, W. and Kafatos, M.: Studying air pollutants origin and associated meteorological parameters over Seoul from 2000 to 2009, Advances in Meteorology, 2015, 704178, doi:10.1155/2015/704178, 2015.

Petzold, A., Kopp, C., and Niessner, R.: The dependence of the specific attenuation cross-section on black carbon mass fraction and particle size, Atmos. Environ., 31, 661–672, 1997.

Prasad A. K., El-Askary, H. M., and Kafatos, M.: Implications of high altitude desert dust transport from Western Sahara to Nile Delta during biomass burning season, Environ. Pollut., 158, 3385–3391, 2010.

Qin, Y. and Mitchell, R. M.: Characterisation of episodic aerosol types over the Australian continent, Atmos. Chem. Phys., 9, 1943–1956, doi:10.5194/acp-9-1943-2009, 2009.

Ramanathan, V., Cess, R. D., Harrison, E. F., Minnis, P., Barkstrom, B. R., Ahmed, E., and Hartmann, D.: Cloud-radiative forcing and climate: Results from the earth radiation budget experiment, Science, 243, 57–63, 1989.

Reid, J. S., Eck, T. F., Christopher, S. A., Hobbs, P. V., and Holben, B.: Use of the Ångstrom exponent to estimate the variability of optical and physical properties of aging smoke particles in Brazil, J. Geophys. Res., 104, 27473–27489, 1999.

Russell, P. B., Bergstrom, R. W., Shinozuka, Y., Clarke, A. D., DeCarlo, P. F., Jimenez, J. L., Livingston, J. M., Redemann, J., Dubovik, O., and Strawa, A.: Absorption Ångstrom Exponent in AERONET and related data as an indicator of aerosol composition, Atmos. Chem. Phys., 10, 1155–1169, doi:10.5194/acp-10-1155-2010, 2010.

Said, S. and Kadry, H.: Generation of representative weather – Year data for Saudi Arabia, Appl. Energ., 48, 131–136, 1994.

Satheesh, S. K. and Moorthy, K. K.: Radiative effects of natural aerosols: A review, Atmos. Environ., 39, 2089–2110, 2005.

Sokolik, I. N. and Toon, O. B.: Incorporation of mineralogical composition into models of the radiative properties of mineral aerosol from UV to IR wavelengths, J. Geophys. Res., 104, 9423–9444, 1999.

Smirnov, A., Holben, B. N., Eck, T. F., Dubovik, O., and Slutsker: Cloud-screening and quality control algorithms for the AERONET database, Remote Sens. Environ., 73, 337–349, 2000.

Smirnov, A., Holben, B. N., Dubovik, O., O'Neill, N. T., Eck, T. F., Westphal, D. L., Goroch, A. K., Pietras, C., and Slutsker, I.: Atmospheric aerosol optical properties in the Persian gulf, J. Atmos. Sci., 59, 620–634, 2002.

Sprigg, W., Nickovic, S., Galgiani, J. N., Pejanovic, G., Petkovic, S., Vujadinovic, M., Vukovic, A., Dacic, M., DiBiase, S., Prasad, A., and El-Askary, H.: Regional dust storm modelling for health services: the case of valley fever, J. of Aeol. Res., 14, 53–73, ISSN 1875-9637, 2014.

Takemura, T., Okamoto, H., Maruyama, Y., Numaguti, A., Higurashi, A., and Nakajima, T.: Global three-dimensional simulation of aerosol optical thickness distribution of various origins, J. Geophys. Res., 105, 17853–17873, 2000.

Taylor, M., Kazadzis, S., Tsekeri, A., Gkikas, A., and Amiridis, V.: Satellite retrieval of aerosol microphysical and optical parameters using neural networks: a new methodology applied to the Sahara desert dust peak, Atmos. Meas. Tech., 7, 3151–3175, doi:10.5194/amt-7-3151-2014, 2014.

Vukovic, A., Vujadinovic, M., Pejanovic, G., Andric, J., Kumjian, M. R., Djurdjevic, V., Dacic, M., Prasad, A. K., El-Askary, H. M., Paris, B. C., Petkovic, S., Nickovic, S., and Sprigg, W. A.: Numerical simulation of "an American haboob", Atmos. Chem. Phys., 14, 3211–3230, doi:10.5194/acp-14-3211-2014, 2014.